Passivating graphene and suppressing interfacial phonon scattering with mechanically transferred large-area Ga2O3

Gebert, M.; Bhattacharyya, S.; Bounds, C.C.; Syed, N.; Daeneke, T.; Fuhrer, M.S.

NANO LETTERS

pubs.acs.org/NanoLett

Letter

Passivating Graphene and Suppressing Interfacial Phonon Scattering with Mechanically Transferred Large-Area Ga_2O_3

Matthew Gebert, Semonti Bhattacharyya,* Christopher C Bounds, Nitu Syed, Torben Daeneke, and Michael S. Fuhrer*

Cite This: *Nano Lett.* 2023, 23, 363−370

Read Online

ACCESS | Metrics & More | Article Recommendations | Supporting Information

ABSTRACT: We demonstrate a large-area passivation layer for graphene by mechanical transfer of ultrathin amorphous Ga_2O_3 synthesized on liquid Ga metal. A comparison of temperature-dependent electrical measurements of millimeter-scale passivated and bare graphene on SiO_2/Si indicates that the passivated graphene maintains its high field effect mobility desirable for applications. Surprisingly, the temperature-dependent resistivity is reduced in passivated graphene over a range of temperatures below 220 K, due to the interplay of screening of the surface optical phonon modes of the SiO_2 by high-dielectric-constant Ga_2O_3 and the relatively high characteristic phonon frequencies of Ga_2O_3. Raman spectroscopy and electrical measurements indicate that Ga_2O_3 passivation also protects graphene from further processing such as plasma-enhanced atomic layer deposition of Al_2O_3.

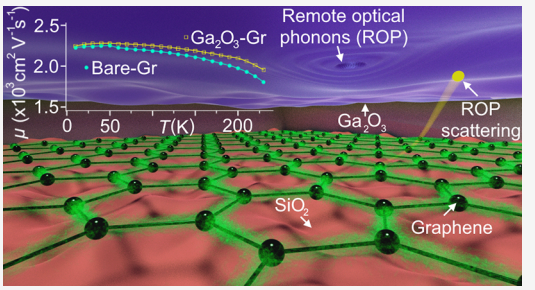

KEYWORDS: *"chemical vapor deposition (CVD) graphene", "mm-scale oxide dielectric", "passivation", "remote interfacial polar phonon scattering", "van der Waals heterostructure", "dielectric screening"*

Insulating layers are essential components of van der Waals heterostructures[1]—isolating materials electronically, passivating them, and enabling electrostatic gating. High-quality hexagonal boron nitride (h-BN), hand-exfoliated from small single crystals, has been widely used as a wide bandgap insulator for vdW heterostructures, enabling exceptional device quality.[2−5]

However, the growth of large area hBN is limited to mainly chemical vapor deposition growth on metal, which requires large-scale infrastructure, or high-purity costly metal rendering the process neither cost-effective nor user-friendly.[6−8] In addition, hBN grown in this method can only be transferred on graphene through a wet-chemical process that can contaminate the heterostructure. This may cause difficulties with industrial-scale applications of hBN[9,10] prompting a search for other suitable insulators to enable large-area vdW heterostructures.

In the case of encapsulating graphene, optimizing the material is highly complex; graphene's electronic properties are largely determined by the insulator's properties, including charged impurity concentration,[11] dielectric constant,[12] and surface optical (SO) phonons which remotely scatter carriers in the graphene,[13,14] and trade-offs exist, e.g., insulators with intermediate dielectric constants may be optimal.[15]

Recently, the surface of liquid metals has been used to synthesize large-area atomically thin materials with facile mechanical transfer onto other substrates through a cost- and user-friendly process that does not require very high temperature, costly catalysts, toxic chemicals, or feedstock gases.[6,16−19] Indeed, Ga_2O_3 has already been shown to be (i) an effective gate dielectric[20] and (ii) an excellent encapsulating layer for transition metal dichalcogenide crystals (TMDs),[21] preserving and even enhancing their optical properties.

Here we investigate liquid-metal synthesized Ga_2O_3 as a large-area encapsulating layer for graphene with an intermediate relative static dielectric constant $\kappa \sim 10$.[22] We mechanically transfer large-area (millimeter-scale) Ga_2O_3 onto one portion of a millimeter-scale graphene-on-SiO_2 device, allowing us to compare the electronic transport properties of bare and Ga_2O_3-encapsulated portions of the same device. We find that coating graphene with Ga_2O_3 preserves the charge carrier mobility close to 3000 $cm^2\ V^{-1}\ s^{-1}$. Surprisingly, we observe a reduction in temperature-dependent resistivity at temperatures below 220 K in the graphene encapsulated by the Ga_2O_3 dielectric, explained by the interplay of screening of the SO phonon modes of the SiO_2 by high-dielectric-constant Ga_2O_3 and the relatively high characteristic phonon frequencies of Ga_2O_3 itself. We further show that Ga_2O_3 is useful as a passivation layer, protecting against damage from deposition of Al_2O_3 via plasma enhanced ALD.

Received: September 4, 2022
Revised: November 3, 2022
Published: November 21, 2022

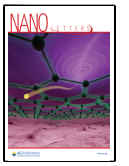

https://doi.org/10.1021/acs.nanolett.2c03492
Nano Lett. 2023, 23, 363−370

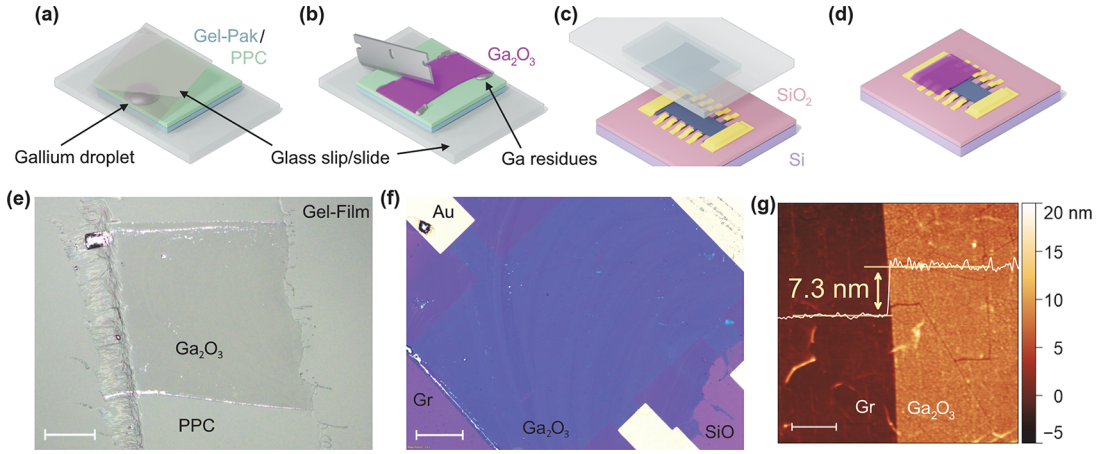

Figure 1. Characterization of Ga_2O_3 thin film transferred on Gr (CVD-grown monolayer graphene/monolayer h-BN film on SiO_2). Schematic representation of (a) gallium metal positioned to be rolled across a PPC/Gel-Pak polymer stack using a coverslip, (b) Ga_2O_3 after rolling with some gallium metal residues, which can be cut away by a razor, (c) transfer of Ga_2O_3 film onto Gr/SiO_2/Si device, and (d) device after removing polymer residues. (e) Optical darkfield micrograph of Ga_2O_3 on PPC after cutting to size. The silver colored dots are liquid gallium droplets. The Ga_2O_3 sheet at the center is bordered by liquid gallium. The scale bar is 200 μm. (f) Brightfield optical micrograph of Ga_2O_3 (deep blue sheet on the device) transferred on a Gr-device. The scale bar is 50 μm. (g) Topographic image of Ga_2O_3-on-Gr sheet obtained by intermittent contact atomic force microscopy (AFM). The left side of the image shows bare Gr, and right side of the image shows Ga_2O_3-covered Gr. Mean height difference is 7.3 nm as shown in the overlaid line profile, and the scalebar is 2 μm.

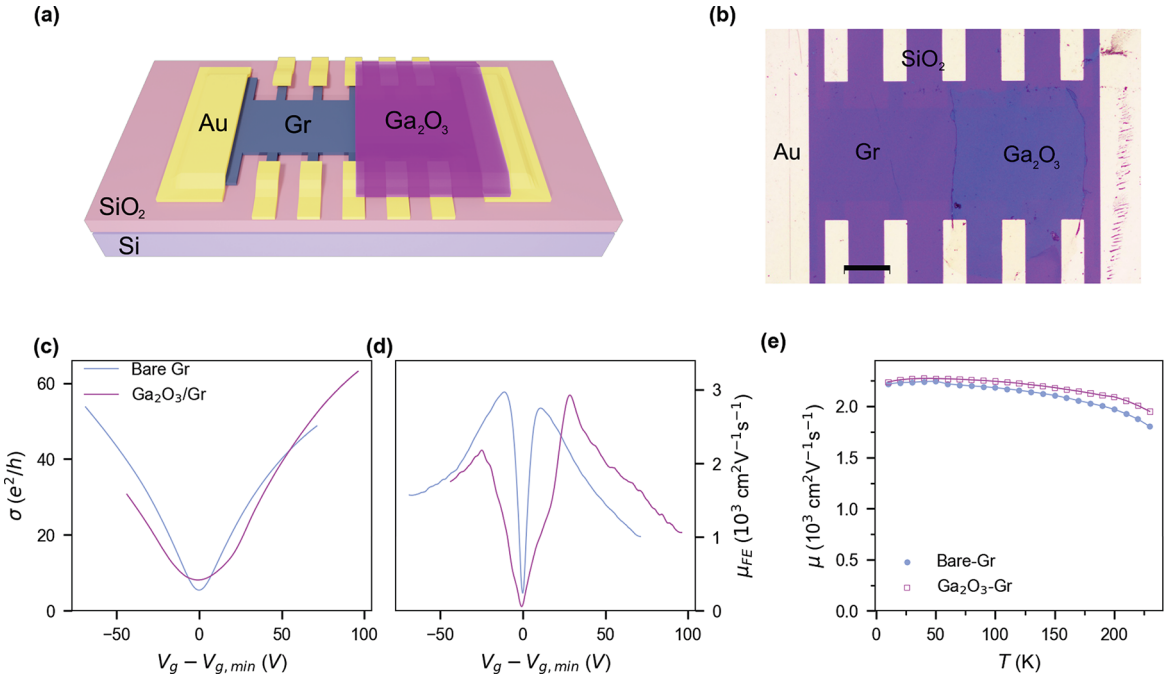

Figure 2. Gate voltage and temperature dependent electrical transport measurements of Ga_2O_3-covered and bare Gr field effect devices. (a) Schematic illustration and (b) optical microscope image of a Gr-device after Ga_2O_3 transfer. The scale bar is 200 μm. (c) Longitudinal conductivity σ and (d) field-effect mobility μ_{FE} as a function of gate voltage V_g offset by gate voltage at minimum conductivity $V_{g,min}$, for both bare Gr and Ga_2O_3-covered Gr at 100 K. (e) Temperature- (T-) dependent effective mobility (μ) calculated at charge carrier density $n = 5 \times 10^{12}$ cm^{-2}.

Devices were fabricated (see Sections S1 and S2, Supporting Information) using a commercial (Graphene Supermarket[23]) CVD-grown monolayer graphene/monolayer h-BN film (henceforth referred to as "Gr") already transferred onto a 285 nm SiO_2/Si (p-doped) substrate that functions as a global back-gate dielectric and electrode. The Gr was then etched into a Hall bar geometry 0.4 mm wide and 1.2 mm long, with multiple voltage electrodes spaced by 0.25 mm, and contacted by Ti/Au electrodes fabricated using conventional photolithography. Next, millimeter-scale ultrathin Ga_2O_3 was prepared on a PPC film on a PDMS stamp (Gel-film, Gelpak) through a liquid metal "squeeze-printing"[19] technique. Finally, Ga_2O_3 was deterministically transferred onto half of the Gr device.[21] We compare the experimental signatures of "bare" and "Ga_2O_3-covered" parts of graphene in the same Hall bar device to understand the effect of Ga_2O_3.

Figure 1 illustrates the steps in the construction of the Ga_2O_3-on-Gr device. The process of transferring ultrathin Ga_2O_3 films on such Gr-devices is schematically represented in Figure 1a–d. First, a mm-scale ultrathin Ga_2O_3 film was

https://doi.org/10.1021/acs.nanolett.2c03492
Nano Lett. 2023, 23, 363−370

prepared on a PPC film mounted on a PDMS stamp through a liquid metal printing technique known as "squeeze-printing"[19] (Figure 1a). This film was then cut into appropriate size to cover half of the Gr-device as well as to get rid of additional Ga-particles (Figure 1b), and was finally deterministically transferred onto half of the Gr Hall bar device using a homemade van der Waals stacking set up[21] (Figure 1, parts c and d).

Figure 1e shows a dark-field image of a squeeze-printed Ga_2O_3 film on PPC/PDMS assembly. This film was trimmed to 0.7 mm × 0.65 mm to match the Gr-device. The darkfield image highlights the Ga-metal residue, left from the squeeze-printing processs, which is negligible in the interior area of the film, and mostly appears at the boundary. Figure 1f shows a bright-field optical image of the Ga_2O_3 film transferred on the Gr-device. The optical contrast of the amorphous Ga_2O_3 film is largely uniform, though slight variations are visible, indicating similar thickness across the thin film (Section S9, Supporting Information). Figure 1g shows an atomic force micrograph of both Ga_2O_3-covered (right-half) and bare side (left-half) of a Gr-device. The AFM line profile (overlaid) yields a step height of 7.3 nm for Ga_2O_3, similar to AFM measurements performed on similar devices (Section S9, Supporting Information), and consistent with thicknesses reported by Wurdack et al.[21]

Figure 2 compares the gate-voltage and temperature dependent electrical transport properties of the bare and Ga_2O_3-covered Gr-devices. The 3D schematic of the device and top-view micrograph are shown in Figure 2, parts a and b, respectively. Figure 2b shows that the transferred Ga_2O_3 film covers half of the Gr-device. The orientation of the Ga_2O_3 film has been carefully controlled so that the Ga-metal particles at the boundary do not affect the electrical transport characteristics between the voltage probes.

Figure 2c shows the gate voltage (V_g) dependence of the longitudinal conductivity σ measured at temperature T = 100 K for both bare and Ga_2O_3-covered Gr. The gate voltage V_g is offset by the gate voltage of minimum conductivity ($V_{g,min}$ = −1.2 and −26.2 V respectively for the bare and Ga_2O_3-covered sides) to facilitate comparison between the two sides of the device. The comparison of the two parts of the sample shows three notable differences, with the Ga_2O_3-covered part showing (i) slightly enhanced conductivity at high V_g, (ii) increased magnitude of minimum conductivity σ_{min}, and (iii) a broader minimum−conductivity plateau.

In order to highlight the first of these features we plot the field effect mobility ($\mu_{FE} = \frac{1}{c_g}\frac{\partial\sigma}{\partial V_g}$; c_g = capacitance of the SiO_2 back gate) obtained from $\sigma(V_g)$ data (Figure 2d). The peak electron mobility is slightly improved in the Ga_2O_3-covered graphene (μ_{FE} = 2900 $cm^2\ V^{-1}\ s^{-1}$) relative to bare graphene (μ_{FE} = 2800 $cm^2\ V^{-1}\ s^{-1}$). The highest observed hole mobility in Ga_2O_3-covered Gr (μ_{FE} = 2200 $cm^2\ V^{-1}\ s^{-1}$) is lower than in bare Gr (μ_{FE} = 3000 $cm^2\ V^{-1}\ s^{-1}$) but might not be a global maximum, as it is at the edge of the V_g measurement window. μ_{FE} is observed to be mostly unchanged by the addition of Ga_2O_3, if not a little increased at high positive V_g.

To understand whether the changes in mobility are due to Ga_2O_3 passivation and are reproducible, we have measured 60 additional devices, 30 with Ga_2O_3 passivation and 30 without; the detailed results are shown in Supporting Information, Section S11. We found that with the addition of Ga_2O_3, room temperature electron mobility μ_e increased by 47.7 ± 15.0% and hole mobility μ_h decreased by 52.2 ± 4.4% (See Supporting Information, Figure S6). Due to the greater importance of remote optical phonon scattering at room temperature (see below) a quantitative comparison is difficult, but the room-temperature observations are qualitatively similar to that seen in Figure 2d at 100 K. Control devices processed identically but without Ga_2O_3 passivation showed smaller changes (3.8 ± 12.1% decrease in μ_e and 18.4 ± 7.9% increase in μ_h) which are likely due to cleaning and annealing.

The slight enhancement of mobility after deposition of Ga_2O_3 is remarkable because previous experiments found that deposition of oxide usually degrades the mobility of graphene[24] due to introduction of disorder. In contrast, screening by a clean dielectric can reduce charged impurity scattering.[12,25] To infer the impurity concentration in SiO_2/Gr/Ga_2O_3 with RPA-Boltzmann theory,[26] we use κ = 10 for the amorphous Ga_2O_3[22] and μ = 2900 $cm^2\ V^{-1}\ s^{-1}$ and calculate an impurity concentration of n_{imp,Ga_2O_3} = 3.8 × 10^{12} cm^{-2} (Section S6.A in the Supporting Information), roughly twice the impurity concentration inferred for our bare graphene on SiO_2 ($n_{imp,bare}$ = 1.8 × 10^{12} cm^{-2}). This indicates that our liquid-metal synthesized and mechanically transferred Ga_2O_3 layer has low charged impurity concentration, comparable to thermally grown SiO_2.

According to the RPA-Boltzmann theory, the increased n_{imp} should also lead to a very weak reduction of σ_{min}[26] and a narrowing of the minimum conductivity plateau in the Ga_2O_3-covered graphene (Section S6.B in the Supporting Information), in contrast to our observation (Figure 2c). The increased σ_{min}, as well as broadening of the minimum conductivity plateau, likely instead reflects additional macroscopic inhomogeneity of the sample[27] induced by the Ga_2O_3.

In order to further explore the modification of electrical transport in Ga_2O_3-covered graphene, we plotted the effective mobility $\mu = \frac{\sigma}{ne}$ calculated at n = 5 × 10^{12} cm^{-2} for both bare and Ga_2O_3-covered graphene (Figure 2e). We observe a gradual reduction in mobility with increasing temperature between 60 and ≈220 K in both. The overall decline of mobility indicates a temperature-dependent resistivity contribution, which surprisingly appears larger in bare compared to Ga_2O_3-covered graphene, in contrast to previous experiments where addition of an oxide layer on graphene increased the temperature-dependent resistivity.[28]

We expect that dielectric layers affect the temperature dependent mobility of graphene through scattering of charge carriers by SO phonons. This process, also known as remote optical phonon (ROP) scattering, is expected to contribute a resistivity proportional to a Bose−Einstein distribution.[14]

$$\rho_{ROP}(V_g, T) = V_g^{-\alpha}\sum_i^M \frac{\beta_i}{e^{\hbar\omega_i/k_BT} - 1} \quad (1)$$

Here the ith SO mode is described by the SO phonon energy $\hbar\omega^i$ (meV) and respective coupling strength β_i (V_g^{α}). Empirically, the dependence on gate voltage is found to follow a power law with $\alpha \approx 1$.

To examine the differences in ROP scattering for bare and Ga_2O_3-covered graphene, we extracted $\rho_{ROP}(V_g,T)$ from $\rho(V_g,T)$ (see Section S10, Supporting Infromation for details). Briefly, we perform a global fit of $\rho(V_g,T)$ at different V_g at 70 K ≤ T ≤ 100 K to determine the acoustic phonon scattering contribution $\rho_{LA}(T)$, which is linear in temperature and independent of V_g, and the impurity contribution $\rho_{imp}(V_g, T$ =

https://doi.org/10.1021/acs.nanolett.2c03492
Nano Lett. 2023, 23, 363−370

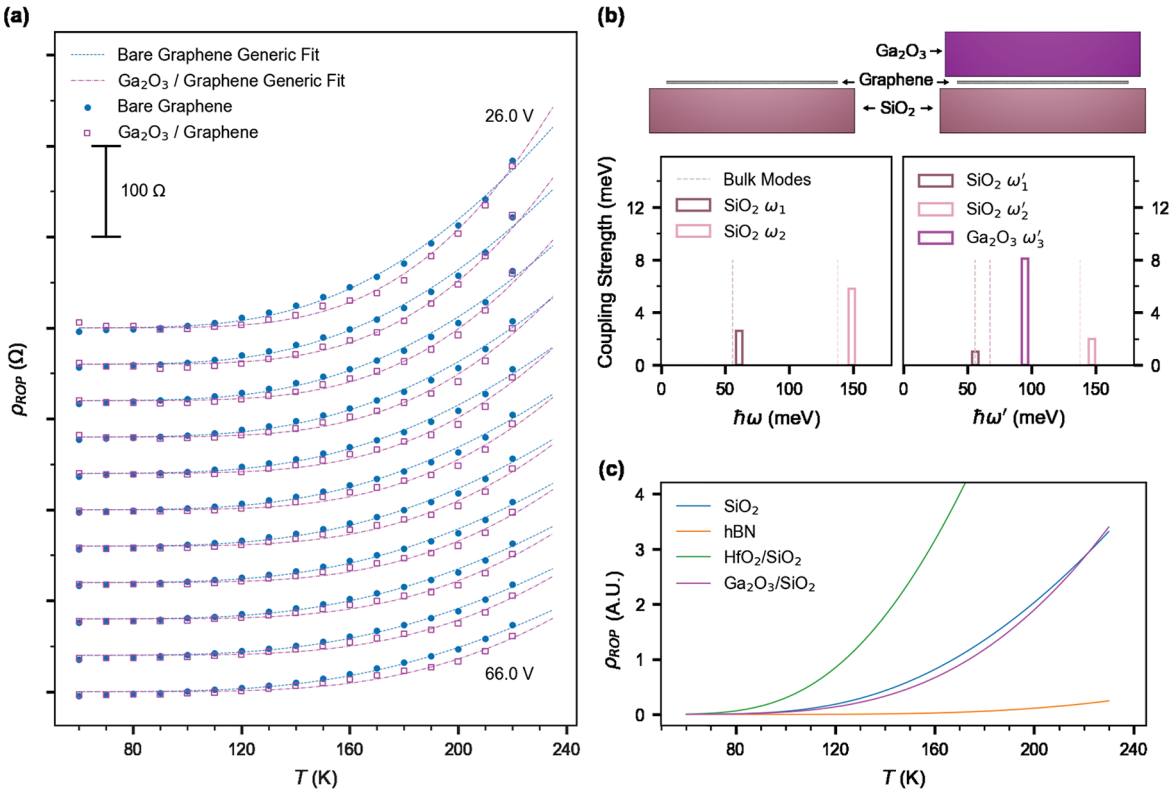

Figure 3. Remote optical phonon (ROP) scattering. (a) ROP contributions to resistivity (ρ_{ROP}) extracted from the temperature- (T-) dependence of resistivity (ρ) in bare (filled) and Ga_2O_3-covered (hollow) graphene. Fits using eq 1 are plotted with dashed line for bare and dot-dashed line Ga_2O_3-covered Gr. For each gate voltage, from 26 through 66 V via 4 V steps, ρ_{ROP} is offset by 40 Ω. (b) Computed frequency and coupling strength of SO phonons in bare and Ga_2O_3-covered Gr. Dashed lines indicate the corresponding bulk mode phonon frequency. (c) Modeled ROP scattering contribution to the resistivity (ρ_{ROP}) in graphene for different dielectric systems.

0 K), which depends on V_g but not temperature. Subtracting these two quantities from $\rho(V_g,T)$ allows us to extract $\rho_{ROP}(V_g, T)$.

Figure 3a shows the contribution of ROP scattering $\rho_{ROP}(V_g, T)$ to resistivity as a function of temperature, for various positive gate voltages (offset from the minimum $V_{g,min}$). $\rho_{ROP}(V_g, T)$ increases superlinearly in temperature, with larger magnitude at smaller $V_g - V_{g,min}$. Remarkably, in the temperature range 70−220 K, ρ_{ROP} is lower in the Ga_2O_3-covered Gr compared to bare Gr for all values of $V_g - V_{g,min}$. The dashed lines in Figure 3a are global fits of the data to eq 1 for a single phonon mode (M = 1) for bare (dashed) and Ga_2O_3-covered (dot-dash) graphene.

The results of the fits in Figure 3a are summarized in Table 1. We determine the SO mode energy, $\hbar\omega_0$, to be larger in

Table 1. Parameters for Fits of Data in Figure 3 for Bare and Ga_2O_3-Covered Graphene to Equation 1

	α	β ($V^{-\alpha}$ h/e^2)	$\hbar\omega_0$ (meV)
Bare	0.97 ± 0.03	6.0 ± 1.1	69.5 ± 1.3
Ga_2O_3	1.18 ± 0.03	43.1 ± 6.7	92.8 ± 2.6

Ga_2O_3-covered graphene (92.8 meV) compared to bare graphene on SiO_2 (69.5 meV). The observation of slightly higher $\hbar\omega_0$ compared to the expected lowest phonon mode for SiO_2 (61 meV) was also observed by Chen et al.,[14] and it is likely due to the additional contribution of the higher-energy SiO_2 mode. The power-law exponent α is similar for bare and Ga_2O_3-covered graphene and close to that of the previous literature.[14,28] The coupling strength β is found to be 6.0 (h/e^2) for bare graphene, which is roughly double the value of 3.26 (h/e^2) found by Chen et al.[14] Due to the different values of α for Ga_2O_3-covered graphene, it is difficult to directly compare the coupling β, which has different dimensions and consequently has a different magnitude to that for bare graphene.

Our observations (Table 1) indicate that the smaller magnitude of $\rho_{ROP}(V_g, T)$ at low temperatures ($T \lesssim 220$ K) for Ga_2O_3-covered graphene is due to a higher effective phonon energy, resulting in a lower $\rho_{ROP}(V_g, T)$ at low temperatures due to lower phonon population, and eventually crossing over to higher $\rho_{ROP}(V_g, T)$ at high T due to stronger coupling. To better understand the lower ρ_{ROP} contribution in Ga_2O_3-covered graphene, we develop a simple analytical model of the SiO_2/graphene/Ga_2O_3 heterostructure, following the methodology used in semiconductor inversion layers[29] and graphene systems.[13,28] The details of the model are described in Section S8 of the Supporting Information.

The resultant phonon frequencies and coupling constants of both bare and Ga_2O_3-covered graphene is schematically represented in Figure 3b (see Tables S2 and S3−S6, Supporting Information, for more details). We find that the graphene/SiO_2 structure has two SO modes, i.e., $\hbar\omega_1$ = 61 meV and $\hbar\omega_2$ = 149 meV. The Ga_2O_3/graphene/SiO_2 structure has three SO modes, with energies and coupling strengths shown in Figure 3b. Here $\hbar\omega_1'$ = 56 meV, $\hbar\omega_2'$ = 147 meV are the perturbed SiO_2 modes, while $\hbar\omega_3'$ = 95 meV originates in Ga_2O_3. While all these modes are thermally activated, the Ga_2O_3 mode couples particularly strongly, also

https://doi.org/10.1021/acs.nanolett.2c03492
Nano Lett. 2023, 23, 363−370

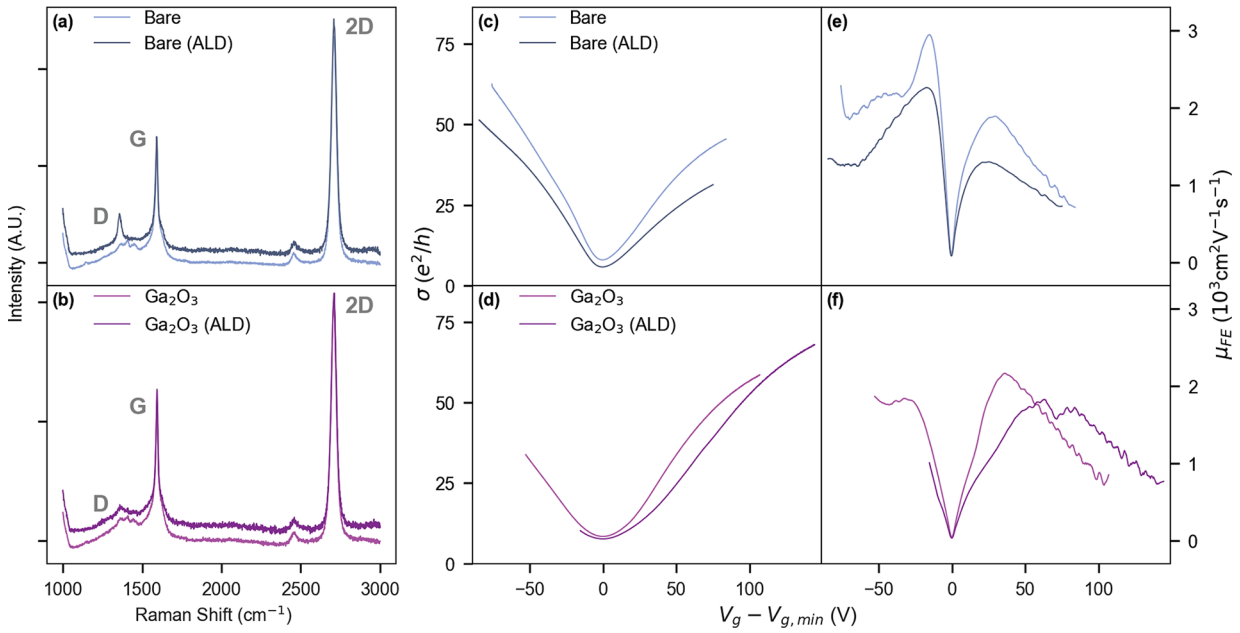

Figure 4. Ga_2O_3 as a protective layer on graphene against plasma-enhanced atomic layer deposition (ALD) of Al_2O_3. Raman spectroscopy with D, G, and 2D peaks indicated for (a) bare graphene and (b) Ga_2O_3-covered graphene. Gate-dependence of conductivity (σ) and field-effect mobility (μ_{FE}) respectively for (c, e) bare Gr and (d, f) Ga_2O_3-covered Gr. Data is shown for the same samples before (lighter shade) and after (darker shade) of the ALD process. Raman and transport data are taken from different samples at room temperature.

reflected in the high disparity between $\epsilon^0_{Ga_2O_3}$ and $\epsilon^\infty_{Ga_2O_3}$ (Table S2 and Section S8, Supporting Information). At the same time, however, the large $\epsilon^\infty_{Ga_2O_3}$ screens the ROP scattering from SiO_2 modes. Hence we expect the ω_3' mode to dominate the temperature-dependent resistivity. Importantly, the energy corresponding to the ω_3' mode matches well with the $\hbar\omega_0$ value obtained from fitting our experimental data (Figure 3a) and Table 1.

Figure 3c shows the analytically obtained $\rho_{ROP}(T)$ for the Ga_2O_3/graphene/SiO_2 structure and bare graphene/SiO_2 calculated using eq 1, using the SO modes as shown in Figure 3c (also given in Table S3 and Table S6, Supporting Information). Also shown for comparison are graphene/h-BN, and HfO_2/graphene/SiO_2 (Tables S4 and S5, Supporting Information). We see that $\rho_{ROP}(T)$ in Ga_2O_3/graphene/SiO_2 is lower than for bare graphene/SiO_2 at temperatures below approximately 220 K. Because ROP is thermally activated, at low temperatures the SiO_2 mode (ω_1) dominates ρ_{ROP} for bare graphene/SiO_2, while for the Ga_2O_3/graphene/SiO_2 structure, the Ga_2O_3 effectively screens these SiO_2 contributions. At higher T, the Ga_2O_3 ROP scattering with higher mode energy ($\omega_3' > \omega_1'$) becomes active and quickly begins to dominate due to the higher coupling. Our observation that addition of Ga_2O_3 to graphene/SiO_2 can lower the overall interfacial phonon scattering may inspire the design of other heterostructures to further reduce scattering phenomena of charge carriers in graphene, perhaps yielding a more significant improvement at or above room temperature.

In our model, we have ignored the effect of the monolayer h-BN in between graphene and SiO_2. The experimental data agree well with our model, and this is consistent with previous ROP experimental models in graphene on SiO_2.[14,28] This might be surprising because one might expect the hBN monolayer crystal to play a significant role in determining the ROP scattering in graphene. However, the experimental results suggest otherwise. These results suggest that the surface modes of h-BN/SiO_2 are comparable to that of bare SiO_2; however, further work is needed to understand why that is the case. This may be explained by the similar dielectric constants of the SiO_2 and h-BN resulting in similar SO properties for the monolayer h-BN/SiO_2 composite to bare SiO_2. Our model on SiO_2/graphene/HfO_2 device matches with previous results as expected.[28]

Having demonstrated that Ga_2O_3 does not enhance impurity scattering in graphene and even reduces the impact of phonon scattering in a certain temperature range, we now investigate whether Ga_2O_3 is effective in protecting graphene from further processing. Methods of growing large-area dielectric films, such as CVD, atomic layer deposition (ALD), sputtering, and e-beam evaporation, have proven to be damaging for graphene, leading to enhancement of impurity scattering and consequently degradation of mobility.[28,30−34]

Our gentle transfer technique for thin Ga_2O_3 avoids such damaging processes, as demonstrated in Figure 2. We further demonstrate the protective nature of Ga_2O_3 by using plasma-enhanced ALD to grow a 5.5 nm layer of Al_2O_3 over the entire sample, following the method of Tang et al.[31] (see Section S3, Supporting Information, for further details), in order to replicate conditions that normally might damage graphene. The ALD chamber temperature is modified to 150 °C, to avoid possible change of morphology of amorphous Ga_2O_3 by thermal annealing.[21]

Figure 4 compares the effect of Al_2O_3 deposition on the bare and the Ga_2O_3-covered side of the Gr device. Parts a and b of Figure 4 show Raman spectra on bare and Ga_2O_3-covered sides respectively before and after ALD deposition. Both areas of the device show monolayer graphene G and 2D Raman peaks at 1591 and 2709 cm^{-1}, with expected ratio ∼2. Before ALD deposition the graphene spectra on both sides are nearly identical, confirming that Ga_2O_3-transfer process does not lead to any structural disorder in graphene. However, there is a

https://doi.org/10.1021/acs.nanolett.2c03492
Nano Lett. 2023, 23, 363−370

stark difference between the Raman spectra on both sides of the devices after ALD processing, where the bare graphene area shows a fully formed D-peak (1357 cm^{-1}), which is nearly absent in preprocessed graphene and remains unchanged in the Ga_2O_3-covered graphene even after processing. The D peak is activated by point disorder and indicates deposition-induced damage in bare graphene, which is not present in Ga_2O_3-covered graphene. This clearly indicates that the Ga_2O_3 transfer has no adverse effect on graphene, and it also acts as an encapsulating layer to protect graphene against further damage during subsequent deposition processes.

This is further supported through electrical transport data obtained on both sides of an identically prepared device before and after Al_2O_3 deposition (Figure 4c–f). Figure 4c,d and Figure 4e,f show the relative change in σ and μ_{FE} respectively before and after ALD, both on bare and Ga_2O_3-covered graphene. After ALD processing, there is a global decrease in σ and μ_{FE} for bare graphene, and peak μ_{FE} drops by ≈30%, compared to >15% in Ga_2O_3-covered graphene. At higher gate voltages ($V_g - V_{g,min} > 50$ V) the transport in processed Ga_2O_3-covered graphene shows similar performance to prior to ALD, with higher μ_{FE} values, and similar σ at ≈100 V. The broadening (and slight reduction) of the μ_{FE} peak in the Ga_2O_3-covered side (Figure 4f) appears to have been caused by further enhancement of the inhomogeneity already present in the system, as the higher mobility at high carrier density indicates that ALD on Ga_2O_3-covered graphene does not induce additional impurities, in agreement with the Raman spectroscopy results.

We checked the reproducibility of Ga_2O_3 passivation as a protective layer using the 60 additional devices previously discussed (Supporting Information, Section S11). After deposition of Al_2O_3 via ALD on Ga_2O_3 passivated and bare devices, we find that the Ga_2O_3 passivation provided significant protection of mobility for both electron (12.0 ± 11.0% increase) and hole carriers (5.6 ± 13.6% increase; see Supporting Information, Figure S7). After ALD, the bare devices underwent a large reduction in hole mobility (42.7 ± 7.9%), while electron mobility varied greatly (net 16.9 ± 28% increase), indicating more disorder compared to Ga_2O_3-covered samples, similar to the effects seen in Figure 2.

Our results demonstrate that liquid-metal synthesized Ga_2O_3 is a viable large-area mechanically transferred passivation layer for vdW heterostructures. Encapsulation of graphene by Ga_2O_3 preserves the mobility, and reduces ROP scattering in graphene below T = 220 K due to the interplay of high energy phonon modes and dielectric screening in this oxide with intermediate dielectric constant. The large area passivation capability of Ga_2O_3 enables other deposition methods without causing damage at the interface, which should allow integration with a variety of materials and processes. The liquid metal printing technique is highly versatile with a wide range of materials already demonstrated;[19] hence, this work opens the possibility of expanding to other liquid metal printed ultrathin materials for large-area vdW heterostructures.

■ ASSOCIATED CONTENT

Supporting Information

The Supporting Information is available free of charge at https://pubs.acs.org/doi/10.1021/acs.nanolett.2c03492.

Device fabrication, mechanical transfer of Ga_2O_3, atomic layer deposition (ALD) of Al_2O_3, electrical measurements in PPMS and probe station, Raman spectroscopy, self-consistent theory for graphene's conductivity, temperature-dependence of the hysteresis of $\sigma - V_g$ in bare graphene and Ga_2O_3-covered graphene, remote optical phonon (ROP) scattering model, Ga_2O_3 atomic-force and darkfield microscopy, extraction of ρ_{ROP} as a function of temperature, additional devices to assess reproducibility of changes in transport properties after Ga_2O_3 passivation and ALD, and Figures S1–S8 (PDF)

■ AUTHOR INFORMATION

Corresponding Authors

Semonti Bhattacharyya − *School of Physics and Astronomy, Monash University, Melbourne, Victoria 3800, Australia; ARC Centre of Excellence in Future Low-Energy Electronics Technologies, Monash University, Melbourne, Victoria 3800, Australia; Leiden Institute of Physics, Leiden University, 2333 CA Leiden, The Netherlands;* orcid.org/0000-0003-3387-0531; Email: bhattacharyya@physics.leidenuniv.nl

Michael S. Fuhrer − *School of Physics and Astronomy, Monash University, Melbourne, Victoria 3800, Australia; ARC Centre of Excellence in Future Low-Energy Electronics Technologies, Monash University, Melbourne, Victoria 3800, Australia;* orcid.org/0000-0001-6183-2773; Email: michael.fuhrer@monash.edu

Authors

Matthew Gebert − *School of Physics and Astronomy, Monash University, Melbourne, Victoria 3800, Australia; ARC Centre of Excellence in Future Low-Energy Electronics Technologies, Monash University, Melbourne, Victoria 3800, Australia;* orcid.org/0000-0003-1363-9498

Christopher C Bounds − *School of Physics and Astronomy, Monash University, Melbourne, Victoria 3800, Australia*

Nitu Syed − *School of Physics, The University of Melbourne, Parkville, Melbourne, Victoria 3010, Australia; School of Engineering, RMIT University, Melbourne, Victoria 3000, Australia*

Torben Daeneke − *School of Engineering, RMIT University, Melbourne, Victoria 3000, Australia; ARC Centre of Excellence in Future Low-Energy Electronics Technologies, RMIT University, Melbourne, Victoria 3000, Australia;* orcid.org/0000-0003-1142-8646

Complete contact information is available at: https://pubs.acs.org/10.1021/acs.nanolett.2c03492

Notes

The authors declare no competing financial interest.

■ ACKNOWLEDGMENTS

This work was supported by the ARC Centre of Excellence in Future Low-Energy Electronics Technologies (CE170100039). We acknowledge Dr. Kaijian Xing for discussions regarding the dielectric constant of Ga_2O_3 and Dr. Matthias Wurdack for discussions regarding the transfer process of Ga_2O_3. Dr. Nitu Syed acknowledges the Mackenzie Fellowship for funding and support. This work was performed in part at the Melbourne Centre for Nanofabrication (MCN) in the Victorian Node of the Australian National Fabrication Facility (ANFF) with

support from Mark Edmonds' ANFF-VIC Technology Fellowship.

REFERENCES

(1) Novoselov, K. S.; Mishchenko, A.; Carvalho, A.; Castro Neto, A. H. 2D materials and van der Waals heterostructures. *Science* **2016**, *353*, aac9439.
(2) Dean, C. R.; Young, A. F.; Meric, I.; Lee, C.; Wang, L.; Sorgenfrei, S.; Watanabe, K.; Taniguchi, T.; Kim, P.; Shepard, K. L.; Hone, J. Boron nitride substrates for high-quality graphene electronics. *Nat. Nanotechnol.* **2010**, *5*, 722−726.
(3) Mayorov, A. S.; Gorbachev, R. V.; Morozov, S. V.; Britnell, L.; Jalil, R.; Ponomarenko, L. A.; Blake, P.; Novoselov, K. S.; Watanabe, K.; Taniguchi, T.; Geim, A. K. Micrometer-Scale Ballistic Transport in Encapsulated Graphene at Room Temperature. *Nano Lett.* **2011**, *11*, 2396−2399.
(4) Xue, J.; Sanchez-Yamagishi, J.; Bulmash, D.; Jacquod, P.; Deshpande, A.; Watanabe, K.; Taniguchi, T.; Jarillo-Herrero, P.; LeRoy, B. J. Scanning tunnelling microscopy and spectroscopy of ultra-flat graphene on hexagonal boron nitride. *Nat. Mater.* **2011**, *10*, 282−285.
(5) Decker, R.; Wang, Y.; Brar, V. W.; Regan, W.; Tsai, H.-Z.; Wu, Q.; Gannett, W.; Zettl, A.; Crommie, M. F. Local electronic properties of graphene on a BN substrate via scanning tunneling microscopy. *Nano Lett.* **2011**, *11*, 2291−2295.
(6) Zavabeti, A.; Jannat, A.; Zhong, L.; Haidry, A. A.; Yao, Z.; Ou, J. Z. Two-Dimensional Materials in Large-Areas: Synthesis, Properties and Applications. *Nano-Micro Lett.* **2020**, *12*, 66.
(7) Li, L.; Zhang, Y.; Zhang, R.; Han, Z.; Dong, H.; Yu, G.; Geng, D.; Yang, H. Y. A minireview on chemical vapor deposition growth of wafer-scale monolayer h-BN single crystals. *Nanoscale* **2021**, *13*, 17310−17317.
(8) Juma, I. G.; Kim, G.; Jariwala, D.; Behura, S. K. Direct growth of hexagonal boron nitride on non-metallic substrates and its heterostructures with graphene. *iScience* **2021**, *24*, 103374.
(9) Novoselov, K. S.; Fal'ko, V. I.; Colombo, L.; Gellert, P. R.; Schwab, M. G.; Kim, K. A roadmap for graphene. *Nature* **2012**, *490*, 192−200.
(10) Ferrari, A. C.; Bonaccorso, F.; Fal'ko, V.; Novoselov, K. S.; Roche, S.; Bøggild, P.; Borini, S.; Koppens, F. H. L.; Palermo, V.; Pugno, N.; Garrido, J. A.; Sordan, R.; Bianco, A.; Ballerini, L.; Prato, M.; Lidorikis, E.; Kivioja, J.; Marinelli, C.; Ryhanen, T.; Morpurgo, A.; Coleman, J. N.; Nicolosi, V.; Colombo, L.; Fert, A.; Garcia-Hernandez, M.; Bachtold, A.; Schneider, G. F.; Guinea, F.; Dekker, C.; Barbone, M.; Sun, Z.; Galiotis, C.; Grigorenko, A. N.; Konstantatos, G.; Kis, A.; Katsnelson, M.; Vandersypen, L.; Loiseau, A.; Morandi, V.; Neumaier, D.; Treossi, E.; Pellegrini, V.; Polini, M.; Tredicucci, A.; Williams, G. M.; Hee Hong, B.; Ahn, J.-H.; Min Kim, J.; Zirath, H.; van Wees, B. J.; van der Zant, H.; Occhipinti, L.; Di Matteo, A.; Kinloch, I. A.; Seyller, T.; Quesnel, E.; Feng, X.; Teo, K.; Rupesinghe, N.; Hakonen, P.; Neil, S. R. T.; Tannock, Q.; Löfwander, T.; Kinaret, J. Science and technology roadmap for graphene, related two-dimensional crystals, and hybrid systems. *Nanoscale* **2015**, *7*, 4598−4810.
(11) Chen, J.-H.; Jang, C.; Adam, S.; Fuhrer, M. S.; Williams, E. D.; Ishigami, M. Charged-impurity scattering in graphene. *Nat. Phys.* **2008**, *4*, 377−381.
(12) Jang, C.; Adam, S.; Chen, J.-H.; Williams, E. D.; das Sarma, S.; Fuhrer, M. S. Tuning the Effective Fine Structure Constant in Graphene: Opposing Effects of Dielectric Screening on Short- and Long-Range Potential Scattering. *Phys. Rev. Lett.* **2008**, *101*, 146805.
(13) Fratini, S.; Guinea, F. Substrate-limited electron dynamics in graphene. *Phys. Rev. B* **2008**, *77*, 195415.
(14) Chen, J.-H.; Jang, C.; Xiao, S.; Ishigami, M.; Fuhrer, M. S. Intrinsic and extrinsic performance limits of graphene devices on SiO_2. *Nat. Nanotechnol.* **2008**, *3*, 206−209.
(15) Konar, A.; Fang, T.; Jena, D. Effect of high-κ gate dielectrics on charge transport in graphene-based field effect transistors. *Phys. Rev. B* **2010**, *82*, 115452.
(16) Zavabeti, A.; Ou, J. Z.; Carey, B. J.; Syed, N.; Orrell-Trigg, R.; Mayes, E. L. H.; Xu, C.; Kavehei, O.; O'Mullane, A. P.; Kaner, R. B.; Kalantar-zadeh, K.; Daeneke, T. A liquid metal reaction environment for the room-temperature synthesis of atomically thin metal oxides. *Science* **2017**, *358*, 332−335.
(17) Kalantar-zadeh, K.; Ou, J. Z.; Daeneke, T.; Mitchell, A.; Sasaki, T.; Fuhrer, M. S. Two dimensional and layered transition metal oxides. *Appl. Mater. Today* **2016**, *5*, 73−89.
(18) Daeneke, T.; Khoshmanesh, K.; Mahmood, N.; de Castro, I. A.; Esrafilzadeh, D.; Barrow, S. J.; Dickey, M. D.; Kalantar-zadeh, K. Liquid metals: fundamentals and applications in chemistry. *Chem. Soc. Rev.* **2018**, *47*, 4073−4111.
(19) Aukarasereenont, P.; Goff, A.; Nguyen, C. K.; McConville, C. F.; Elbourne, A.; Zavabeti, A.; Daeneke, T. Liquid metals: an ideal platform for the synthesis of two-dimensional materials. *Chem. Soc. Rev.* **2022**, *51*, 1253.
(20) Xing, K.; Aukarasereenont, P.; Rubanov, S.; Zavabeti, A.; Creedon, D. L.; Li, W.; Johnson, B. C.; Pakes, C. I.; McCallum, J. C.; Daeneke, T.; Qi, D.-C. Hydrogen-Terminated Diamond MOSFETs Using Ultrathin Glassy Ga_2O_3 Dielectric Formed by Low-Temperature Liquid Metal Printing Method. *ACS Appl. Electron. Mater.* **2022**, *4*, 2272−2280.
(21) Wurdack, M.; Yun, T.; Estrecho, E.; Syed, N.; Bhattacharyya, S.; Pieczarka, M.; Zavabeti, A.; Chen, S.-Y.; Haas, B.; Muller, J.; Lockrey, M. N.; Bao, Q.; Schneider, C.; Lu, Y.; Fuhrer, M. S.; Truscott, A. G.; Daeneke, T.; Ostrovskaya, E. A. Ultrathin Ga_2O_3 Glass: A Large-Scale Passivation and Protection Material for Monolayer WS2. *Adv. Mater.* **2021**, *33*, 2005732.
(22) Passlack, M.; Hunt, N. E. J.; Schubert, E. F.; Zydzik, G. J.; Hong, M.; Mannaerts, J. P.; Opila, R. L.; Fischer, R. J. Dielectric properties of electron-beam deposited Ga_2O_3 films. *Appl. Phys. Lett.* **1994**, *64*, 2715−2717.
(23) Catalog item: CVD Graphene Film/CVD h-BN Film Heterostructure on SiO_2/Si wafer.
(24) Liao, L.; Duan, X. Graphene-Dielectric Integration for Graphene Transistors. *Materials Science and Engineering. R, Reports: a review journal* **2010**, *70*, 354−370.
(25) Newaz, A.K.M.; Puzyrev, Y. S.; Wang, B.; Pantelides, S. T.; Bolotin, K. I. Probing charge scattering mechanisms in suspended graphene by varying its dielectric environment. *Nat. Commun.* **2012**, *3*, 734.
(26) Adam, S.; Hwang, E. H.; Galitski, V. M.; Das Sarma, S. A self-consistent theory for graphene transport. *Proc. Natl. Acad. Sci. U. S. A.* **2007**, *104*, 18392−18397.
(27) Blake, P.; Yang, R.; Morozov, S. V.; Schedin, F.; Ponomarenko, L. A.; Zhukov, A. A.; Nair, R. R.; Grigorieva, I. V.; Novoselov, K. S.; Geim, A. K. Influence of metal contacts and charge inhomogeneity on transport properties of graphene near the neutrality point. *Solid State Commun.* **2009**, *149*, 1068−1071.
(28) Zou, K.; Hong, X.; Keefer, D.; Zhu, J. Deposition of High-Quality HfO_2 on Graphene and the Effect of Remote Oxide Phonon Scattering. *Phys. Rev. Lett.* **2010**, *105*, 126601.
(29) Fischetti, M. V.; Neumayer, D. A.; Cartier, E. A. Effective electron mobility in Si inversion layers in metal−oxide-semiconductor systems with a high-κ insulator: The role of remote phonon scattering. *J. Appl. Phys.* **2001**, *90*, 4587−4608.
(30) Fallahazad, B.; Kim, S.; Colombo, L.; Tutuc, E. Dielectric thickness dependence of carrier mobility in graphene with HfO_2 top dielectric. *Appl. Phys. Lett.* **2010**, *97*, 123105.
(31) Tang, X.; Reckinger, N.; Poncelet, O.; Louette, P.; Ureña, F.; Idrissi, H.; Turner, S.; Cabosart, D.; Colomer, J.-F.; Raskin, J.-P.; Hackens, B.; Francis, L. A. Damage evaluation in graphene underlying atomic layer deposition dielectrics. *Sci. Rep.* **2015**, *5*, 13523.
(32) Jin, Z.; Su, Y.; Chen, J.; Liu, X.; Wu, D. Study of AlN dielectric film on graphene by Raman microscopy. *Appl. Phys. Lett.* **2009**, *95*, 233110.
(33) Dlubak, B.; Seneor, P.; Anane, A.; Barraud, C.; Deranlot, C.; Deneuve, D.; Servet, B.; Mattana, R.; Petroff, F.; Fert, A. Are Al_2O_3

https://doi.org/10.1021/acs.nanolett.2c03492
Nano Lett. 2023, 23, 363−370

and MgO tunnel barriers suitable for spin injection in graphene? *Appl. Phys. Lett.* **2010**, *97*, 092502.
(34) Maneshian, M. H; Kuo, F.-L.; Mahdak, K.; Hwang, J.; Banerjee, R.; Shepherd, N. D The influence of high dielectric constant aluminum oxide sputter deposition on the structure and properties of multilayer epitaxial graphene. *Nanotechnology* **2011**, *22*, 205703.

https://doi.org/10.1021/acs.nanolett.2c03492
Nano Lett. 2023, 23, 363−370